Prolate-shape dominance in atomic nuclei within the deformed relativistic Hartree-Bogoliubov theory in continuum

P. Guo (郭鹏) ⓞ, C. Pan (潘琮) ⓞ,* Y. C. Zhao (赵英淳), X. K. Du (杜晓凯) ⓞ, and S. Q. Zhang (张双全) ⓞ†

State Key Laboratory of Nuclear Physics and Technology, School of Physics, Peking University, Beijing 100871, China

The dominance of prolate over oblate ground-state deformations has been a well-known empirical fact. With the state-of-the-art deformed relativistic Hartree-Bogoliubov theory in continuum (DRHBc) and taking Te, Xe, and Ba isotopes with neutron number $82 \leqslant N \leqslant 126$ as examples, a self-consistent and microscopic study of the prolate-shape dominance is given. According to the calculated potential-energy curves, most of these isotopes have both prolate and oblate minima and prefer prolate in the ground state, while the small amount of oblate ground-state shapes mainly appear after the major shell is half filled. It is also found that the prolate-shape dominance enhances with the proton number increasing from 52 to 56. The dominance and its enhancement can be well understood by the microscopic canonical single-particle energies obtained in the DRHBc theory, in good agreement with the schematic interpretation based on the Nilsson diagram. Finally, pairing correlations are found to bring more energy displacements to oblate minima on average but do not play a decisive role in prolate-shape dominance.

I. INTRODUCTION

It has been a well-known empirical fact that vast majority of deformed nuclei are prolate rather than oblate [1]. Besides the overwhelming dominance of prolate over oblate, another interesting characteristic of nuclear ground-state deformation is that these few oblate nuclei mainly appear near the very end of a major shell. This intriguing prolate-shape dominance has attracted extensive attention and discussion [2–26].

In the textbook of Casten [14], he outlined an inspiring understanding on the origin of the prolate-shape dominance from the simple perspective of a Nilsson diagram. The relative angular orientations of different K orbitals and the specific sequence of single-particle j shells are two essential points. The former results in the fact that there are more downsloping orbitals with low K values on the prolate side than the downsloping orbitals with high K values on the oblate side. The latter makes low K orbitals from different j shells come together on the prolate side and interact, thus lowering the lowest orbitals further.

To address the origin of the prolate-shape dominance more quantitatively, many different approaches have been employed. Tajima *et al.* have performed systematic Skyrme Hartree-Fock plus BCS calculations on the ground states of even-even nuclei and found the overwhelming prolate-shape dominance in the nuclear region with $N > 50$, which was suggested owing to the change of the nature of the major shells from the harmonic-oscillator shell to the Mayer-Jensen shell [12]. In Ref. [18], Hamamoto and Mottelson

compared the system's total energies defined as the sum of the lowest-lying single-particle energies obtained from pure harmonic-oscillator and spheroidal infinite-well potentials. By the comparisons, they emphasized the importance of the surface of one-body potentials and commented that the spin-orbit potential alone cannot affect the prolate-shape dominance. Within the framework of the Nilsson-Strutinsky method, it is found that the synergism of the surface effect and the spin-orbit potential has influence on the prolate-shape dominance [15]. This study has been extended to the Woods-Saxon potential, where the role of the spin-orbit potential is further addressed [21,22]. Recently, the proxy-SU(3) model has been applied to investigate the prolate-shape dominance and it turns out that prolate-dominance can be understood within this algebraic model [24,26].

Pairing correlations are of significance in the description of nuclear ground-state properties. From a general point of view, pairing correlations would enhance the dominance of prolate over oblate, as oblate minima with relatively smaller deformations more easily become spherical under pairing correlations [18]. However, the numerical results based on the Strutinsky shell-correction method showed that pairing correlations have different influences under different parameter conditions [16,22]. In some cases pairing correlations may enhance prolate-shape dominance whereas in others they may have preference for oblate ones.

The covariant density functional theory (CDFT), which includes the Lorentz invariance from the very beginning, has been a powerful method for its successful descriptions of many nuclear phenomena [27–35]. Based on the CDFT, in order to properly consider the continuum effect in a microscopic and self-consistent way, the relativistic continuum Hartree-Bogoliubov (RCHB) theory was developed in

---

*cpan18@pku.edu.cn
†sqzhang@pku.edu.cn

Refs. [36,37] with the relativistic Hartree-Bogoliubov (RHB) equations solved in the coordinate space. Inheriting the advantages of RCHB theory and including the deformation degree of freedom, the deformed relativistic Hartree-Bogoliubov theory in continuum (DRHBc) was developed in Refs. [38,39] with the deformed RHB equations solved in a Dirac Woods-Saxon basis [40,41]. Both the RCHB and DRHBc theories can treat the stable and exotic nuclei in a unified manner and have achieved great success, such as Refs. [36,42–50] and Refs. [51–67]. Very recently, based on the point-coupling density functional PC-PK1 [68], the DRHBc mass table for even-even nuclei has been constructed [69,70], and the table for odd-A and odd-odd nuclei is under construction [71]. From the DRHBc mass table, one can easily find the dominance of the prolate shape over the oblate shape [70]. Therefore, it is interesting to probe the prolate-shape dominance within the state-of-the-art microscopic DRHBc theory. Besides, many investigations on the prolate-shape dominance of stable nuclei have been performed. With the DRHBc theory, it is possible for us to further probe the prolate-shape dominance of more unstable nuclei near the drip line.

In this paper, we take Te, Xe, and Ba isotopes with neutron numbers in the major shell $82 \leqslant N \leqslant 126$ as examples. In this nuclear region, a typical prolate-shape dominance for both even-even nuclei and odd-A nuclei will be presented with the DRHBc calculations. The single-particle energies in the canonical basis will be given to further understand the dominance. To figure out the contributions of pairing effects, the calculated results with and without pairing correlations will be compared.

II. THEORETICAL FRAMEWORK

The details of the DRHBc theory can be found in Refs. [38,39,69,71]. Here only a brief introduction is presented. In the DRHBc theory, the mean field and pairing correlations are treated self-consistently by the relativistic Hartree-Bogoliubov (RHB) equation [72],

$$
\begin{pmatrix} \hat{h}_D - \lambda_\tau & \hat{\Delta} \\ -\hat{\Delta}^* & -\hat{h}_D^* + \lambda_\tau \end{pmatrix} \begin{pmatrix} U_k \\ V_k \end{pmatrix} = E_k \begin{pmatrix} U_k \\ V_k \end{pmatrix}, \qquad (1)
$$

where $\hat{h}_D$ is the Dirac Hamiltonian, λ_τ is the Fermi energy of neutron or proton ($\tau = n, p$), Δ is the pairing potential, E_k is the quasiparticle energy, and U_k and V_k are the quasiparticle wave functions. In the coordinate space,

$$
h_D(\boldsymbol{r}) = \boldsymbol{\alpha} \cdot \boldsymbol{p} + V(\boldsymbol{r}) + \beta[M + S(\boldsymbol{r})], \qquad (2)
$$

where M is the nucleon mass, and $S(\boldsymbol{r})$ and $V(\boldsymbol{r})$ are scalar and vector potentials, respectively. The pairing potential Δ reads

$$
\Delta(\boldsymbol{r}_1, \boldsymbol{r}_2) = V^{pp}(\boldsymbol{r}_1, \boldsymbol{r}_2) \kappa(\boldsymbol{r}_1, \boldsymbol{r}_2), \qquad (3)
$$

where κ is the pairing tensor [73] and V^{pp} is a density-dependent zero-range pairing force,

$$
V^{pp}(\boldsymbol{r}_1, \boldsymbol{r}_2) = V_0 \frac{1}{2}(1 - P^\sigma)\delta(\boldsymbol{r}_1 - \boldsymbol{r}_2)\left(1 - \frac{\rho(\boldsymbol{r}_1)}{\rho_{\text{sat}}}\right). \quad (4)
$$

For an axially deformed nucleus with spatial reflection symmetry, the potentials and densities are expanded in terms of the Legendre polynomials,

$$
f(\boldsymbol{r}) = \sum_\lambda f_\lambda(r) P_\lambda(\cos\theta), \quad \lambda = 0, 2, 4, \dots, \lambda_{\max}. \quad (5)
$$

For an exotic nucleus whose Fermi energy is close to the continuum threshold, the continuum effect induced by pairing scattering could make nucleon density more diffuse in spatial distribution. To properly consider the continuum effect, the deformed RHB equations (1) should be solved in coordinate space with a large box or coordinate-like space. In the DRHBc theory [38,39], one adopts the spherical Dirac Woods-Saxon basis, in which the radial wave functions have a proper asymptotic behavior for large r.

After self-consistently solving the RHB equations, the total energy E_{tot}, quadrupole deformation β_2, and other expectation values can be calculated. The total energy of a nucleus is

$$
\begin{aligned}
E_{\text{RHB}} = {} & E_{\text{nucleon}} + E_{\text{pair}} \\
& - \int d^3\boldsymbol{r} \left(\frac{1}{2}\alpha_S \rho_S^2 + \frac{1}{2}\alpha_V \rho_V^2 + \frac{1}{2}\alpha_{TV}\rho_3^2 \right. \\
& + \frac{2}{3}\beta_S \rho_S^3 + \frac{3}{4}\gamma_S \rho_S^4 + \frac{3}{4}\gamma_V \rho_V^4 + \frac{1}{2}\delta_S \rho_S \Delta\rho_S \\
& \left. + \frac{1}{2}\delta_V \rho_V \Delta\rho_V + \frac{1}{2}\delta_{TV}\rho_3 \Delta\rho_3 + \frac{1}{2}\rho_p e A^0 \right) + E_{\text{c.m.}},
\end{aligned}
$$
$$(6)$$

where the nucleon energy E_{nucleon} reads

$$
E_{\text{nucleon}} = \sum_{k>0}(\lambda - E_k)v_k^2 - 2E_{\text{pair}}, \qquad (7)
$$

with

$$
v_k^2 = \int d^3\boldsymbol{r} V_k^\dagger(\boldsymbol{r})V_k(\boldsymbol{r}). \qquad (8)
$$

The pairing energy E_{pair}, with the zero-range pairing force, is calculated by

$$
E_{\text{pair}} = -\frac{1}{2}\int d^3\boldsymbol{r} \kappa(\boldsymbol{r})\Delta(\boldsymbol{r}). \qquad (9)
$$

The center-of-mass (c.m.) correction energy is calculated by

$$
E_{\text{c.m.}} = -\frac{\langle \hat{\boldsymbol{P}}^2 \rangle}{2MA}, \qquad (10)
$$

where A is the mass number, and $\hat{\boldsymbol{P}} = \sum_i^A \hat{\boldsymbol{p}}_i$ is the total momentum in the c.m. frame [74–76]. The quadrupole deformation is calculated by

$$
\beta_{\tau,2} = \frac{\sqrt{5\pi}Q_{\tau,2}}{3N_\tau \langle r_\tau^2 \rangle}, \qquad (11)
$$

where $Q_{\tau,2}$ is the intrinsic quadrupole moment:

$$
Q_{\tau,2} = \sqrt{\frac{16\pi}{5}}\langle r^2 Y_{20}(\theta, \phi)\rangle. \qquad (12)
$$

The canonical basis is obtained by diagonalizing the density matrix ρ [73],

$$
\rho|\psi_i\rangle = v_i^2|\psi_i\rangle, \qquad (13)
$$

where the eigenvalue v_i^2 is the corresponding occupation probability of $|\psi_i\rangle$. Due to the axial and spatial reflection symmetries, the third component K of the angular momentum and parity π are good quantum numbers to characterize the canonical single-particle levels.

For an odd-A or odd-odd nucleus, the blocking effect of the unpaired nucleon(s) needs to be considered. Here the blocking effect is included with the equal filling approximation [77,78]. More details can be found in Refs. [71,78].

III. NUMERICAL DETAILS

In this paper, we focus our DRHBc investigations for prolate-shape dominance on the Te, Xe, and Ba nuclei with the neutron number belonging to one major shell, i.e., $82 \leqslant N \leqslant 126$. In the corresponding DRHBc calculations, the numerical conditions determined for constructing a global mass table as presented in Refs. [69,71] are used. For the particle-hole channel, the relativistic density functional PC-PK1 [68] is adopted and for the particle-particle channel, the density-dependent zero-range pairing force in Eq. (4) is used, with the pairing strength $V_0 = -325$ MeV fm^3, the saturation density $\rho_{\text{sat}} = 0.152$ fm^{-3} and the cutoff energy in the quasiparticle space 100 MeV for the pairing window. To guarantee the convergence accuracy, the energy cutoff $E_{\text{cut}}^+ = 300$ MeV and the angular-momentum cutoff $J_{\text{max}} = (23/2)\hbar$ for the Dirac Woods-Saxon basis are used. Note that the number of states in the Dirac sea is taken to be the same as that in the Fermi sea [38–40]. Moreover, the maximum K value to be considered in the deformed single-particle orbitals is equal to the value of J_{max}. In Refs. [79,80] where the deformed relativistic Hartree-Fock-Bogoliubov equations are solved with DWS basis, another truncation quantity $K_{m_{\text{max}}}$ is introduced to represent the number of blocks considered for the orbitals with the maximum K value. The present truncation recipe in our work corresponds to $K_{m_{\text{max}}} = 1$. For the Legendre expansion of the deformed potentials and densities, the Legendre expansion truncation $\lambda_{\text{max}} = 6$ is used.

To make a quantitative analysis of prolate-shape dominance, one needs to find out both the prolate minimum and oblate minimum of a nucleus. To find correct local minima without paying high computational cost, we have performed unconstrained DRHBc calculations with initial deformations $\beta_2 = -0.4, -0.2, 0.0, 0.2, 0.4,$ and 0.6. Then the solution with the lowest total energy corresponds to the ground state, whereas the solution with the lowest total energy at the prolate (oblate) side corresponds to the prolate (oblate) minimum. Constrained calculations have been performed for several selected nuclei and the outcomes for the prolate (oblate) minimum are consistent with the unconstrained calculations, which guarantees the correctness of the selection and the self-consistency of the DRHBc calculations.

IV. RESULTS AND DISCUSSION

A. Evolution of ground-state deformation

The ground-state quadrupole deformation parameters β_2 as functions of the neutron number within the major shell $82 \leqslant N \leqslant 126$ for Te, Xe, and Ba isotopic chains in the

DRHBc calculations are shown in Fig. 1. For Te isotopes, except for the beginning $N = 83$ and 84, the deviation from the spherical shape to the prolate shape after the shell closure $N = 82$ and the increase of the absolute value $|\beta_2|$ before midshell can be clearly seen. After midshell around $N = 100$, $|\beta_2|$ starts to decrease gradually as expected and it suddenly becomes close to zero at $N = 111$. Then the deformation remains small up to the magic number $N = 126$, while the last four odd Te isotopes tend to be slightly prolate. The most striking behavior in the Te isotopic chain is the drastic change from a prolate shape with $\beta_2 = 0.30$ at $N = 101$ to an oblate shape with $\beta_2 = -0.20$ at $N = 102$. Besides the global evolutionary trend, a slight odd-even neutron number dependence of the ground-state deformation in Te isotopes can also be noticed.

Similar to Te, except for ^{140}Ba with $N = 84$, the ground-state deformation parameters for Xe and Ba increase after the shell closure $N = 82$ and reach the maxima near midshell around $N = 100$. The shapes of Xe and Ba also deviate from spherical to prolate at the beginning of the major shell, and change to oblate dramatically. But in comparison with $N = 101$ for Te, the transformation points for Xe and Ba isotopic chains are delayed by 4 and 10 neutrons to $N = 105$ and $N = 111$, respectively. The shapes of Xe and Ba turn back into prolate at $N = 117$ and $N = 115$ again, respectively, and finally return spherical at the edge of the major shell $N = 124$ and $N = 126$. Besides, the slight odd-even neutron number dependence of the ground-state deformation can also be seen in Xe and Ba isotopes. In a word, most of the ground-state shapes of Te, Xe, and Ba prefer prolate after the shell closure $N = 82$, and the small amount of oblate ground-state shapes mainly be found after the major shell is almost half filled.

As clearly reflected in Fig. 1, the number of nuclei with prolate ground-state shapes is significantly larger than oblate one, namely the prolate-shape dominance in the $82 \leqslant N \leqslant 126$ major shell can be self-consistently obtained within the microscopic DRHBc theory. Quantitatively for Te, 36 nuclei are obtained to be deformed with 14 (38.9%) being oblate. For Xe, 11 of 42 (26.2%) deformed nuclei are oblate and, for Ba, only 3 of 41 (7.32%) deformed nuclei are oblate. The decrease of this ratio suggests the enhancement of prolate-shape dominance as the proton number Z increases from 52 to 56. In addition, the delay of the prolate-to-oblate transformation point shown in Fig. 1 also highlights the important role played by proton here.

The evolution of the ground-state deformations, especially the drastic prolate-to-oblate changes mentioned above can be better understood with the potential-energy curves (PECs), which are obtained by the quadrupole deformation constrained DRHBc calculations. The PECs of selected Te, Xe, and Ba isotopes with even $N = 82, 90, \ldots, 122$ and odd $N = 83, 91, \ldots, 123$ are displayed in Fig. 2. As shown, except for a few nuclei near the beginning or the end of the major shell, most nuclei have two local minima with one at the prolate side and the other at the oblate side. For instance, both the PECs of ^{170}Ba and ^{171}Ba have two local minima respectively lying at the prolate and oblate sides, and their energies are close to each other. In ^{170}Ba the oblate minimum is slightly lower, but in ^{171}Ba the prolate one is slightly lower,
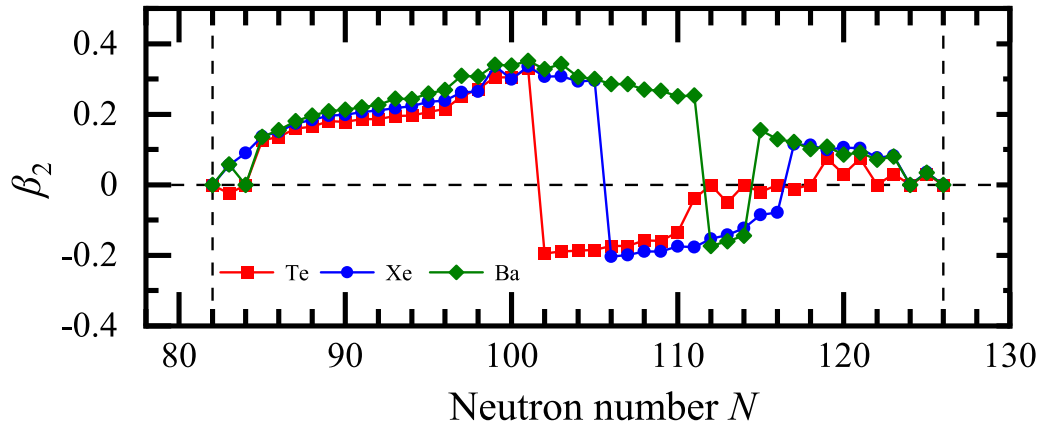
FIG. 1. Quadrupole deformations as functions of the neutron number with $82 \leqslant N \leqslant 126$ for Te (red square), Xe (blue circle), and Ba (green diamond) isotopic chains in the DRHBc calculations with density functional PC-PK1.

corresponding to the sudden change of ground-state shape from oblate to prolate here.

B. Prolate and oblate minima

To further probe the prolate-shape dominance in this nuclear region, it is natural for us to focus on the quadrupole deformation parameters β_2 of the prolate and oblate minima and the energy difference between them, i.e.,

$$E_{\text{diff}} = E_{\text{min}}(\text{oblate}) - E_{\text{min}}(\text{prolate}). \quad (14)$$

For the cases with only one spherical minimum in PECs, e.g., for ^{134,174}Te, we consider it as both prolate and oblate minima and then let $E_{\text{diff}} = 0$.

Figure 3 presents the deformation evolutions of both prolate and oblate minima as well as the energy difference E_{diff} between them obtained in the DRHBc calculations for Te, Xe, and Ba isotopes. As displayed in Fig. 3(a), for most Te isotopes, there exist both prolate and oblate minima. But for the even isotopes ^{134,136}Te at the beginning of and $^{164-178}$Te at the end of the major shell, only the spherical minima are obtained. It is interesting to note their neighboring odd isotopes such as ^{135}Te and $^{165-177}$Te exhibit both prolate and oblate minima with very small $|\beta_2|$ values, which highlights the polarization effect of the odd nucleon. For the remaining isotopes, the $|\beta_2|$ values of both prolate and oblate minima increase with neutron number before the midshell and decreases after the midshell. Most absolute values of β_2 at the prolate side are larger than those at the oblate side. Specif-
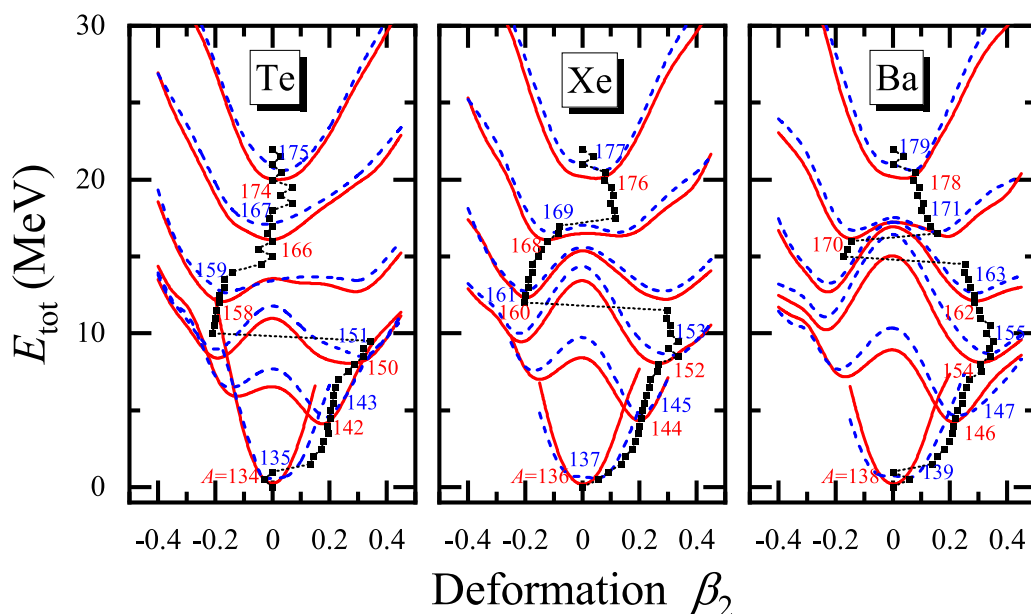

FIG. 2. Evolution of the potential-energy curves of Te, Xe, and Ba isotopes with even $N = 82, 90, \ldots, 122$ (red solid lines) and odd $N = 83, 91, \ldots, 123$ (blue dashed lines). For clarity, in each panel, the PEC of the lightest isotope (^{134}Te, ^{136}Xe, and ^{138}Ba) is renormalized to its ground state, and other PECs are shifted upward by 0.5 MeV per increasing one neutron. The evolution of the ground-state deformation is shown with the black squares.
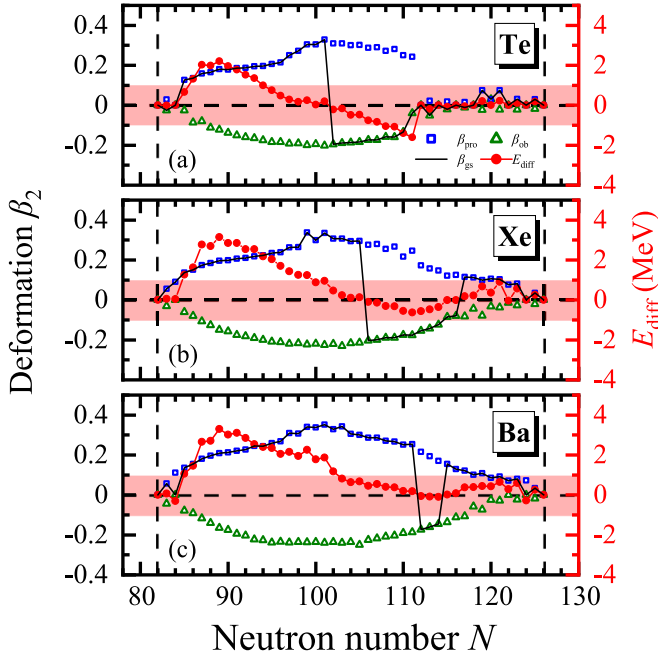
FIG. 3. Quadrupole deformation parameters β_2 of the prolate (blue squares) and oblate (green triangles) minima, as well as the energy difference (red circles) between them $E_{\text{diff}} = E_{\text{min}}(\text{oblate}) - E_{\text{min}}(\text{prolate})$, as functions of the neutron number for Te, Xe, and Ba isotopic chains in the DRHBc calculations with PC-PK1.

ically, the maximum of $|\beta_2|$ of prolate minimum is 0.329, larger than the maximum of $|\beta_2| = 0.202$ at the oblate side. They both reach the maximum at $N = 101$. For the energy difference between the prolate and oblate minima E_{diff}, it can be found that the value increases with neutron number until $E_{\text{diff}} = 2.21$ MeV at $N = 89$ and then decreases, corresponding to the prolate ground states for nuclei before midshell. The E_{diff} alters the sign at $N = 102$, corresponding to the drastic change of ground-state shape to oblate as shown in Fig. 3. The lowest $E_{\text{diff}} = -1.61$ MeV appears at $N = 111$ and then suddenly drops to zero as the nucleus ^{164}Te is spherical. Furthermore, we highlight the region where $|E_{\text{diff}}| \leqslant 1$ MeV to show the nuclei whose prolate and oblate minima have very close energies. It is found that nuclei from ^{146}Te$_{94}$ to ^{159}Te$_{107}$ all have prolate and oblate minima close in energy and with relatively large deformation, indicating that they might be good candidates of shape coexistence.

For Xe and Ba isotopes presented in Figs. 3(b) and 3(c), except for few exceptions like ^{136,178,180}Xe and ^{138,182}Ba, all nuclei have two minima. In consistent with Te isotopes, the $|\beta_2|$ of both prolate and oblate minima increases with neutron number before the midshell and decreases after the midshell, and most $|\beta_2|$ at the prolate side are larger than those at the oblate side. The maxima of $|\beta_2|$ at both prolate and oblate sides also appear around $N = 101$. The evolutionary trends of the E_{diff} curves in Xe and Ba isotopes are similar to Te, i.e., the value increases with neutron number until $N = 89$ and then decreases, corresponding to the prolate ground states for nuclei before midshell. The E_{diff} alters the sign at $N = 106$ for Xe and at $N = 112$ for Ba, respectively, corresponding to
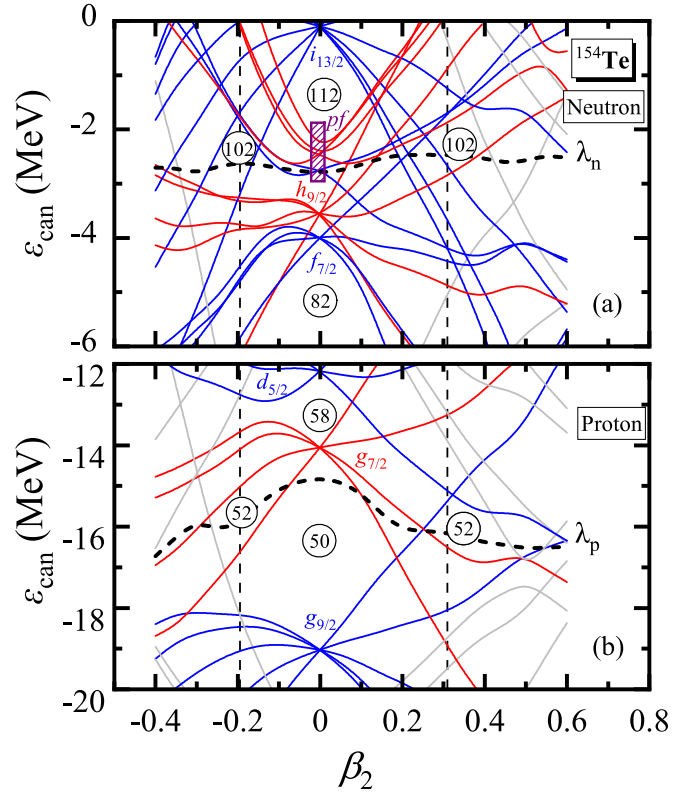

FIG. 4. (a) Single-neutron energies in the canonical basis of ^{154}Te as functions of the deformation parameter β_2 obtained in the DRHBc calculations. The Fermi energy as a function of quadrupole deformation is also displayed by a dashed line. The deformation parameters of the prolate and oblate minima are marked by the vertical dashed lines. The neutron number obtained by filling all the lower levels is shown with a circle at several energy gaps. The spherical subshells l_j are denoted and the pf shell includes $p_{3/2}$, $f_{5/2}$, and $p_{1/2}$. For clarity, the orbitals stemming from the spherical subshell $l_{j=l+1/2}$ are shown in blue and those from the subshell $l_{j=l-1/2}$ are in red. (b) The same as panel (a) but for single-proton energies.

the drastic changes to the oblate ground-state shape. However, E_{diff} alters the sign again at $N = 117$ for Xe and at $N = 115$ for Ba, respectively, which corresponds to the return of the prolate ground-state shape and remarkably shrinks the regime of oblate ground states in comparison with Te. If comparing the E_{diff} in the three isotopic chains quantitatively, it can be found that the E_{diff} for the same N seems to increase as the proton number increases from 52 to 56, that is, the curve of E_{diff} roughly moves up with Z.

C. Canonical single-particle energies

As discussed in the literature, such as Refs. [14,18,25], the prolate-shape dominance is closely related to the underlying single-particle energy spectra on the prolate and oblate sides. To get a further understanding of the origin of the prolate-shape dominance in this nuclear region, it is of particular interest for us to examine the single-particle levels obtained in the self-consistent DRHBc calculations. As an example, Fig. 4 shows the calculated single-particle energies in the

canonical basis as functions of the deformation parameter β_2 for ^{154}Te.

When a nucleus is axially deformed, the total angular momentum j is not a good quantum number any more, but its projection on the symmetry axis K remains a good quantum number. So, as presented in Fig. 4, a j shell in the spherical case will spilt into several K orbitals on the prolate and oblate sides. It is obvious that the splitting of single-particle levels is asymmetric with the prolate-oblate transformation. As seen in Fig. 4(a), the neutron levels near the Fermi energy for ^{154}Te are orbitals stemming from the spherical $f_{7/2}$, pf shell, $h_{9/2}$ as well as the intruder subshell $i_{13/2}$.

From a casual inspection of Fig. 4(a), we can see orbitals with downward slope on both prolate and oblate sides. As is well known, orbitals with low K values tend to go downward on the prolate side whereas high K orbitals have a downward trend on the oblate side. One can notice in Fig. 4(a) that there are more downsloping orbitals on the prolate side than the other side. Generally a high j shell will split more downsloping orbitals on the prolate side than the oblate side. For instance, orbitals with $|K| \leqslant \frac{7}{2}$ from $i_{13/2}$ have a downward slope while only orbitals with $|K| \geqslant \frac{9}{2}$ upward on the prolate side. It stems from the fact that the orientations of the orbital planes change very little for low K values, but increase rapidly for high K [14].

In addition, the lowering of downsloping orbitals due to interactions between low K orbitals can also be found in Fig. 4(a) [14]. Focusing on the lowest $K = \frac{1}{2}$ orbital from $f_{7/2}$ on the prolate side, one notices that it has large downward slope at the beginning and then is pushed still lower due to the interaction with the $K = \frac{1}{2}$ orbital from $h_{9/2}$. Owing to the simple fact that only high j shells have high K orbitals while every subshell in a major shell can split out low K orbitals, the avoided-crossing interactions between the same K orbitals will strengthen the fanning out of the prolate side but reduce the fanning out of the oblate side. This brings an apparent asymmetry in the splitting of single-neutron levels, and finally results in an energetic preference for prolate shape and the emergence of the prolate-shape dominance. Nevertheless, after these strong downsloping orbitals on the prolate side have been filled with $N \approx 102$, a preference for oblate shape may have a chance to develop, producing the occurrence of oblate ground states in the second-half of the major shell. It is interesting to note that, in comparison with the traditional Nilsson diagram [14,73], the DRHBc calculations predict that the positive parity $i_{13/2}$ orbital is the highest spherical subshell within the major shell ($82 \leqslant N \leqslant 126$) instead of in the middle. Still one can see that the lowest three orbitals stemming from $i_{13/2}$ descend so rapidly that they can make contributions to the prolate-shape dominance in this nuclear region. By further increasing N towards 126, the deformation gets close to zero. As seen in Fig. 4, the filling of the orbitals from $i_{13/2}$ would become more important. In this sense, due to the existence of three strongly downsloping orbitals from $i_{13/2}$ on the prolate side, the nucleus would prefer the prolate shape. As a result, the sign of E_{diff} might change again from negative to positive and the oblate to prolate shape transformation appears near the end of the major shell. Investigations on the single-neutron levels for some other Te isotopes as well as Xe and Ba

isotopes have been done and the similarities of shell structure have been identified, which can explain the similarities of the energy displacement E_{diff} presented in Fig. 3.

As seen in Fig. 4(b), the proton levels near the Fermi energy for ^{154}Te are orbitals stemming from the spherical $g_{9/2}$, $g_{7/2}$, and $d_{5/2}$. One can notice that, after the shell closure ($Z = 50$), the lowest spherical shell here is the high-j orbital $g_{7/2}$. Similar to the case presented in Fig. 4(a), the $K = \frac{1}{2}$ orbital stemming from $g_{7/2}$ has a large downward slope due to the interaction with the same $K = \frac{1}{2}$ orbital from $d_{5/2}$. From the single-proton and single-neutron levels in Fig. 4, a possible explanation can also be given on the enhancement of the prolate-shape dominance as proton number increases from 52 to 56. Figure 3 shows that after the shell closure ($N = 82$) with neutron filling downsloping $f_{7/2}$ and $h_{9/2}$ orbitals, E_{diff} increases with neutron number increasing from 84 to 88, indicating more energetic preference for prolate shape. Similar to the case, the filling of protons in the downsloping $g_{7/2}$ orbital after the shell closure ($Z = 50$) can also bring more energetic preference for prolate shape, thus enhancing the prolate-shape dominance as Z increases from 52 to 56.

D. Pairing effects

Pairing correlations are essential in understanding many nuclear properties [73]. Therefore, it is meaningful to study the influence of pairing correlations on the prolate-shape dominance within the self-consistently microscopic DRHBc calculations. Taking Te isotopic chain as an example, Fig. 5 shows the impacts of pairing correlations on the prolate-oblate shape competition, including the influence on the quadrupole deformation parameters of the prolate and oblate minima, on the corresponding binding energies, as well as on the energy difference E_{diff} by comparing the results with and without pairing correlations.

As presented in Fig. 5(a), pairing correlations will in general make $|\beta_2|$ of both prolate and oblate minima become smaller. In particular, at the beginning and end of the major shell, for most nuclei with moderate deformation in the absence of pairing, the inclusion of pairing correlations leads them spherical or nearly spherical. This behavior is what we can expect, as the existence of monopole pairing correlations favors a spherical nuclear shape [73].

Figure 5(b) shows a detailed examination on the total-energy displacements ΔE brought by the pairing correlations for both prolate and oblate minima. All the values of ΔE are non-negative due to the fact that pairing correlations always tend to make nuclei more bound. Also as expected, there appears the obvious odd-even staggering in ΔE, because the blocking of the odd nucleon will reduce the pairing effect and then bring less binding in odd-N nuclei. It can be further noticed that, for a certain nucleus, pairing correlations mainly bring more binding to the oblate minimum than to the prolate minimum; the opposite case seldom happens. Concretely, the average energy displacement brought by the pairing correlations for the oblate minima $\overline{\Delta E} = 1.39$ MeV is larger than $\overline{\Delta E} = 1.01$ MeV for prolate ones. The larger $\overline{\Delta E}$ of the oblate minima might be attributed to the higher energy level densities near the neutron Fermi surface. For example, as presented
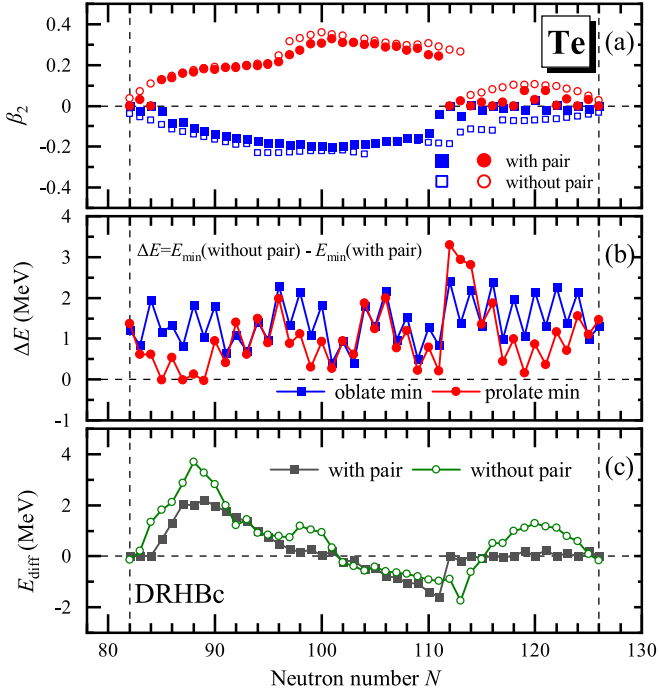
FIG. 5. The impacts of pairing correlations on the prolate-oblate shape competition for Te isotopic chain obtained in the DRHBc calculations with PC-PK1. (a) Quadrupole deformation parameters of the prolate and oblate minima as functions of the neutron number with (solid symbols) or without (open symbols) pairing correlations. (b) Energy difference between the prolate local minima with and without pairing correlations (red circles), and that between the oblate ones (blue squares). (c) Energy difference between the prolate and oblate minima with (black squares) or without (olive circles) pairing correlations.

in Fig. 4, when about 98 neutrons are filled, three single-particle levels very close in energy can be found at $\beta_2 \approx -0.2$, whereas obviously less energy levels appear at $\beta_2 \approx 0.3$. This indicates more energies from pairing effects on the oblate side than the prolate side, which is consistent with the obviously larger energy displacement for oblate minima in the region $97 \leqslant N \leqslant 100$, as shown in Fig. 5(b). Similarly, the obviously larger ΔE in the regions $84 \leqslant N \leqslant 90$ and $116 \leqslant N \leqslant 124$ can be understood from the higher level densities on the oblate side as well.

Figure 5(c) further shows the energy difference between the prolate and oblate minima E_{diff} for Te isotopes obtained by the DRHBc calculations with pairing correlations, in comparison with the corresponding calculations without pairing correlations. As seen, the two curves of E_{diff} are roughly similar to each other and their transformation points from the prolate to oblate ground state are at the same nucleus ^{154}Te. Corresponding to the more binding brought to oblate minima shown in Fig. 5(b), the prolate and oblate minima become more close for many Te isotopes. For the detailed ratio, 16 of 45 (35.6%) deformed nuclei in ground state are oblate when calculated without pairing correlations, in comparison with the aforementioned ratio 14 of 36 (38.9%) when calculated with pairing. These numbers indicate the prolate-shape dominance in Te isotopes gets slightly weakened by considering pairing

correlations. As seen in Fig. 5(a), this weakening is mainly caused by that several prolate nuclei at the end of the major shell become spherical when including pairing correlations.

For Xe and Ba isotopes, we find similar effects of pairing correlations on the prolate and oblate minima, i.e., pairing correlations make $|\beta_2|$ of both prolate and oblate minima become smaller and generally bring more binding to the oblate minima than to the prolate minima. It is also found that 13 of 45 (28.9%) deformed Xe nuclei are oblate when calculated without pairing in comparison with 11 of 42 (26.2%) when with pairing, and 4 of 45 (8.89%) deformed Ba nuclei are oblate when calculated without pairing in comparison with 3 of 41 (7.32%) when with pairing. This means, in contrast with Te, pairing correlations slightly enhance the prolate-shape dominance in Xe and Ba. By examining the energy difference between the prolate and oblate minima, it is found that the enhancement comes from two reasons: (1) As noted in Ref. [18], a few oblate systems with slight deformation become spherical when pairing correlations are included. (2) Although, in general, pairing correlations bring more binding to the oblate minimum than to the prolate minimum, the opposite cases happen occasionally and lead very few oblate systems to become prolate when with pairing. Nevertheless, based on the study of all three chains, one can draw a conclusion that pairing correlations do influence the quantitative ratio of prolate systems to oblate ones but do not play a decisive role in the emergence of prolate-shape dominance.

Finally, it has to be mentioned that the present investigation is in the axially symmetric case. In Ref. [81], by using the triaxial relativistic Hartree-Bogoliubov (TRHB) theory with the same density functional PC-PK1 but with the finite-range separable pairing force, the authors have performed a systemic study of the even-even nuclei with $8 \leqslant Z \leqslant 104$. According to their results, the prolate-shape dominance appears throughout the nuclear landscape. For the Te, Xe, and Ba isotopes studied here, the similarities and differences between present results and those in Ref. [81] are worth noting. In the TRHB calculations, except ^{168}Xe and ^{168,170,172}Ba, all the other isotopes are predicted to be spherical or axially deformed. Both the behavior of prolate-shape dominance and the shape evolutions along with the neutron number are quite similar between the two results, only that in TRHB the prolate-to-oblate transformation points are slightly shifted to $N = 98$ and $N = 106$ for Te and Xe isotopes, respectively, and for Ba isotopes the few oblate ones in DRHBc are replaced by the triaxial ones in TRHB. The displacement of the transformation points can be attributed to the different pairing interactions adopted. Nevertheless, this comparison indicates the inclusion of the triaxial degree of freedom would not break the dominance of prolate over oblate and the main conclusion presented here still holds.

V. SUMMARY

In summary, taking Te, Xe, and Ba isotopes with neutron number in the major shell $82 \leqslant N \leqslant 126$ as examples, the prolate-shape dominance is investigated with the state-of-the-art microscopic DRHBc theory. It is found that most of these isotopes prefer prolate after the shell closure $N = 82$, and the

oblate ground-state shapes mainly appear after the shell is half filled. As the proton number Z increases from 52 to 56, the delay of the prolate-to-oblate transformation point and the enhancement of prolate-shape dominance are shown. According to the calculated potential-energy curves, most studied isotopes have both prolate minimum and oblate minimum, and the drastic prolate-to-oblate transformation corresponds to the strong competition between the two minima. The deformations of oblate and prolate minima and energy difference E_{diff} between them are examined to further probe the prolate-shape dominance. It is shown that prolate minima have overall larger deformations than oblate ones. Additionally, it is found that all three isotopic chains have similar evolutionary trends of the E_{diff} curves and the enhancement of the prolate-shape dominance is revealed by the moving-up of the E_{diff} curve with Z. The prolate-shape dominance and its enhancement are understood through the single-particle levels self-consistently obtained by the DRHBc theory. The dominance can be mainly attributed to more downsloping orbitals in quantity on the prolate side and the interaction between them. Besides, both proton and neutron can play an important role in prolate-shape dominance. The effect of pairing correlations is also examined by the comparison between the results with and without pairing correlations. It is found that though pairing correlations bring more energy displacements to oblate minima in average, they do not play a decisive role in prolate-shape dominance.

In the future, the construction of the DRHBc mass table [70,71] would allow us to investigate the prolate-shape dominance on the whole nuclear chart rather than a specific nuclear region, and in particular one may probe the phenomenon for the vast weakly bound nuclei far away from the β-stability line. In addition, it would be interesting to study the triaxial effects on the prolate-shape dominance by using the newly developed triaxial relativistic Hartree-Bogoliubov theory in continuum [82] and to explore the beyond-mean-field effects by restoring the rotational invariance and considering the shape fluctuations.

[1] A. Bohr and B. R. Mottelson, *Nuclear Structure* (Benjamin, New York, 1975), Vol. II.

[2] E. Teller and J. A. Wheeler, Phys. Rev. **53**, 778 (1938).

[3] W. Rarita and J. Schwinger, Phys. Rev. **59**, 436 (1941).

[4] R. H. Lemmer, Phys. Rev. **117**, 1551 (1960).

[5] R. H. Lemmer and V. F. Weisskopf, Nucl. Phys. **25**, 624 (1961).

[6] K. Kumar, Phys. Rev. C **1**, 369 (1970).

[7] B. Castel and K. Goeke, Phys. Rev. C **13**, 1765 (1976).

[8] W. Zickendraht, Phys. Rev. Lett. **54**, 1906 (1985).

[9] B. Castel, D. Rowe, and L. Zamick, Phys. Lett. B **236**, 121 (1990).

[10] H. Frisk, Nucl. Phys. A **511**, 309 (1990).

[11] I. Hamamoto, B. R. Mottelson, H. Xie, and X. Z. Zhang, Z. Phys. D: At., Mol. Clusters **21**, 163 (1991).

[12] N. Tajima, S. Takahara, and N. Onishi, Nucl. Phys. A **603**, 23 (1996).

[13] K. Arita, A. Sugita, and K. Matsuyanagi, Czech. J. Phys. B **48**, 821 (1998).

[14] R. F. Casten, *Nuclear Structure from a Simple Perspective* (Oxford University Press, Oxford, 2000).

[15] N. Tajima and N. Suzuki, Phys. Rev. C **64**, 037301 (2001).

[16] N. Tajima, Y. R. Shimizu, and N. Suzuki, Prog. Theor. Phys. Suppl. **146**, 628 (2002).

[17] M. A. Deleplanque, S. Frauendorf, V. V. Pashkevich, S. Y. Chu, and A. Unzhakova, Phys. Rev. C **69**, 044309 (2004).

[18] I. Hamamoto and B. R. Mottelson, Phys. Rev. C **79**, 034317 (2009).

[19] M. Horoi and V. Zelevinsky, Phys. Rev. C **81**, 034306 (2010).

[20] P. Stránský, A. Frank, and R. Bijker, J. Phys.: Conf. Ser. **322**, 012018 (2011).

[21] S. Takahara, N. Onishi, Y. R. Shimizu, and N. Tajima, Phys. Lett. B **702**, 429 (2011).

[22] S. Takahara, N. Tajima, and Y. R. Shimizu, Phys. Rev. C **86**, 064323 (2012).

[23] D. Bonatsos, I. E. Assimakis, N. Minkov, A. Martinou, S. Sarantopoulou, R. B. Cakirli, R. F. Casten, and K. Blaum, Phys. Rev. C **95**, 064326 (2017).

[24] D. Bonatsos, Eur. Phys. J. A **53**, 148 (2017).

[25] D. Bonatsos, K. E. Karakatsanis, A. Martinou, T. J. Mertzimekis, and N. Minkov, Phys. Rev. C **106**, 044323 (2022).

[26] M. Sugawara, Phys. Rev. C **106**, 024301 (2022).

[27] P. Ring, Prog. Part. Nucl. Phys. **37**, 193 (1996).

[28] D. Vretenar, A. Afanasjev, G. Lalazissis, and P. Ring, Phys. Rep. **409**, 101 (2005).

[29] J. Meng, H. Toki, S. Zhou, S. Zhang, W. Long, and L. Geng, Prog. Part. Nucl. Phys. **57**, 470 (2006).

[30] T. Nikšić, D. Vretenar, and P. Ring, Prog. Part. Nucl. Phys. **66**, 519 (2011).

[31] J. Meng, J. Peng, S. Q. Zhang, and P. W. Zhao, Front. Phys. **8**, 55 (2013).

[32] J. Meng and S. G. Zhou, J. Phys. G **42**, 093101 (2015).

[33] *Relativistic Density Functional for Nuclear Structure*, edited by J. Meng (World Scientific, Singapore, 2016).

[34] S.-G. Zhou, Phys. Scr. **91**, 063008 (2016).

[35] S. Shen, H. Liang, W. H. Long, J. Meng, and P. Ring, Prog. Part. Nucl. Phys. **109**, 103713 (2019).

[36] J. Meng and P. Ring, Phys. Rev. Lett. **77**, 3963 (1996).

[37] J. Meng, Nucl. Phys. A **635**, 3 (1998).

[38] S.-G. Zhou, J. Meng, P. Ring, and E.-G. Zhao, Phys. Rev. C **82**, 011301(R) (2010).

[39] L. Li, J. Meng, P. Ring, E.-G. Zhao, and S.-G. Zhou, Phys. Rev. C **85**, 024312 (2012).

[40] S.-G. Zhou, J. Meng, and P. Ring, Phys. Rev. C **68**, 034323 (2003).

[41] K. Y. Zhang, C. Pan, and S. Q. Zhang, Phys. Rev. C **106**, 024302 (2022).

[42] J. Meng and P. Ring, Phys. Rev. Lett. **80**, 460 (1998).

[43] J. Meng, I. Tanihata, and S. Yamaji, Phys. Lett. B **419**, 1 (1998).

[44] J. Meng, K. Sugawara-Tanabe, S. Yamaji, P. Ring, and A. Arima, Phys. Rev. C **58**, R628 (1998).

[45] J. Meng, K. Sugawara-Tanabe, S. Yamaji, and A. Arima, Phys. Rev. C **59**, 154 (1999).

[46] J. Meng, H. Toki, J. Y. Zeng, S. Q. Zhang, and S.-G. Zhou, Phys. Rev. C **65**, 041302(R) (2002).

[47] S. Q. Zhang, J. Meng, S. G. Zhou, and J. Y. Zeng, Chin. Phys. Lett. **19**, 312 (2002).

[48] J. Meng, S.-G. Zhou, and I. Tanihata, Phys. Lett. B **532**, 209 (2002).

[49] H. F. Lu, J. Meng, S. Q. Zhang, and S. G. Zhou, Eur. Phys. J. A **17**, 19 (2003).

[50] W. Zhang, J. Meng, S. Q. Zhang, L. S. Geng, and H. Toki, Nucl. Phys. A **753**, 106 (2005).

[51] Y. Chen, L. Li, H. Liang, and J. Meng, Phys. Rev. C **85**, 067301 (2012).

[52] X.-X. Sun, J. Zhao, and S.-G. Zhou, Phys. Lett. B **785**, 530 (2018).

[53] K. Y. Zhang, D. Y. Wang, and S. Q. Zhang, Phys. Rev. C **100**, 034312 (2019).

[54] C. Pan, K. Zhang, and S. Zhang, Int. J. Mod. Phys. E **28**, 1950082 (2019).

[55] X.-X. Sun, J. Zhao, and S.-G. Zhou, Nucl. Phys. A **1003**, 122011 (2020).

[56] E. J. In, P. Papakonstantinou, Y. Kim, and S.-W. Hong, Int. J. Mod. Phys. E **30**, 2150009 (2021).

[57] Z. H. Yang, Y. Kubota, A. Corsi, K. Yoshida, X.-X. Sun, J. G. Li, M. Kimura, N. Michel, K. Ogata, C. X. Yuan, Q. Yuan, G. Authelet, H. Baba, C. Caesar, D. Calvet, A. Delbart, M. Dozono, J. Feng, F. Flavigny, J.-M. Gheller, J. Gibelin *et al.* Phys. Rev. Lett. **126**, 082501 (2021).

[58] X.-X. Sun, Phys. Rev. C **103**, 054315 (2021).

[59] K. Zhang, X. He, J. Meng, C. Pan, C. Shen, C. Wang, and S. Zhang, Phys. Rev. C **104**, L021301 (2021).

[60] C. Pan, K. Y. Zhang, P. S. Chong, C. Heo, M. C. Ho, J. Lee, Z. P. Li, W. Sun, C. K. Tam, S. H. Wong, R. W.-Y. Yeung, T. C. Yiu, and S. Q. Zhang, Phys. Rev. C **104**, 024331 (2021).

[61] X.-T. He, C. Wang, K.-Y. Zhang, and C.-W. Shen, Chin. Phys. C **45**, 101001 (2021).

[62] X.-X. Sun and S.-G. Zhou, Sci. Bull. **66**, 2072 (2021).

[63] X.-X. Sun and S.-G. Zhou, Phys. Rev. C **104**, 064319 (2021).

[64] Y.-B. Choi, C.-H. Lee, M.-H. Mun, and Y. Kim, Phys. Rev. C **105**, 024306 (2022).

[65] S. Kim, M.-H. Mun, M.-K. Cheoun, and E. Ha, Phys. Rev. C **105**, 034340 (2022).

[66] W. Sun, K.-Y. Zhang, C. Pan, X.-H. Fan, S.-Q. Zhang, and Z.-P. Li, Chin. Phys. C **46**, 064103 (2022).

[67] K. Y. Zhang, P. Papakonstantinou, M.-H. Mun, Y. Kim, H. Yan, and X.-X. Sun, Phys. Rev. C **107**, L041303 (2023).

[68] P. W. Zhao, Z. P. Li, J. M. Yao, and J. Meng, Phys. Rev. C **82**, 054319 (2010).

[69] K. Zhang, M.-K. Cheoun, Y.-B. Choi, P. S. Chong, J. Dong, L. Geng, E. Ha, X. He, C. Heo, M. C. Ho, E. J. In, S. Kim, Y. Kim, C.-H. Lee, J. Lee, Z. Li, T. Luo, J. Meng, M.-H. Mun, Z. Niu, C. Pan, P. Papakonstantinou, X. Shang, C. Shen, G. Shen, W. Sun, X.-X. Sun, C. K. Tam, Thaivayongnou, C. Wang, S. H. Wong, X. Xia, Y. Yan, R. W.-Y. Yeung, T. C. Yiu, S. Zhang, W. Zhang, and S.-G. Zhou (DRHBc Mass Table Collaboration), Phys. Rev. C **102**, 024314 (2020).

[70] K. Zhang, M.-K. Cheoun, Y.-B. Choi, P. S. Chong, J. Dong, Z. Dong, X. Du, L. Geng, E. Ha, X.-T. He, C. Heo, M. C. Ho, E. J. In, S. Kim, Y. Kim, C.-H. Lee, J. Lee, H. Li, Z. Li, T. Luo, J. Meng, M.-H. Mun, Z. Niu, C. Pan, P. Papakonstantinou, X. Shang, C. Shen, G. Shen, W. Sun, X.-X. Sun, C. K. Tam, Thaivayongnou, C. Wang, X. Wang, S. H. Wong, J. Wu, X. Wu, X. Xia, Y. Yan, R. W.-Y. Yeung, T. C. Yiu, S. Zhang, W. Zhang, X. Zhang, Q. Zhao, and S.-G. Zhou (DRHBc Mass Table Collaboration), At. Data Nucl. Data Tables **144**, 101488 (2022).

[71] C. Pan, M.-K. Cheoun, Y.-B. Choi, J. Dong, X. Du, X.-H. Fan, W. Gao, L. Geng, E. Ha, X.-T. He, J. Huang, K. Huang, S. Kim, Y. Kim, C.-H. Lee, J. Lee, Z. Li, Z.-R. Liu, Y. Ma, J. Meng, M.-H. Mun, Z. Niu, P. Papakonstantinou, X. Shang, C. Shen, G. Shen, W. Sun, X.-X. Sun, J. Wu, X. Wu, X. Xia, Y. Yan, T. C. Yiu, K. Zhang, S. Zhang, W. Zhang, X. Zhang, Q. Zhao, R. Zheng, and S.-G. Zhou (DRHBc Mass Table Collaboration), Phys. Rev. C **106**, 014316 (2022).

[72] H. Kucharek and P. Ring, Z. Phys. A: Hadrons Nucl. **339**, 23 (1991).

[73] P. Ring and P. Schuck, *The Nuclear Many-Body Problem* (Springer-Verlag, Berlin, 1980).

[74] M. Bender, K. Rutz, P.-G. Reinhard, and J. Maruhn, Eur. Phys. J. A **7**, 467 (2000).

[75] W. Long, J. Meng, N. Van Giai, and S.-G. Zhou, Phys. Rev. C **69**, 034319 (2004).

[76] P.-W. Zhao, B.-Y. Sun, and J. Meng, Chin. Phys. Lett. **26**, 112102 (2009).

[77] S. Perez-Martin and L. M. Robledo, Phys. Rev. C **78**, 014304 (2008).

[78] L.-L. Li, J. Meng, P. Ring, E.-G. Zhao, and S.-G. Zhou, Chin. Phys. Lett. **29**, 042101 (2012).

[79] J. Geng, J. Xiang, B. Y. Sun, and W. H. Long, Phys. Rev. C **101**, 064302 (2020).

[80] J. Geng and W. H. Long, Phys. Rev. C **105**, 034329 (2022).

[81] Y. L. Yang, Y. K. Wang, P. W. Zhao, and Z. P. Li, Phys. Rev. C **104**, 054312 (2021).

[82] K. Y. Zhang, S. Q. Zhang, and J. Meng, arXiv:2212.05703.